10th International Conference on Fracture Mechanics of Concrete and Concrete Structures
FraMCoS-X
G. Pijaudier-Cabot, P. Grassl and C. La Borderie (Eds)

COUPLING STATISTICAL INDENTATION AND MICROSCOPY TO EVALUATE MICROMECHANICAL PROPERTIES OF CEMENTITIOUS MATERIALS

B. HILLOULIN, M. ROBIRA AND A. LOUKILI

Institut de Recherche en Génie Civil et Mécanique (GeM), UMR-CNRS 6183,Ecole Centrale de Nantes, 1 rue de la Noe, 44321 Nantes.

Benoit.Hilloulin@ec-nantes.fr
Maxime.Robira@ec-nantes.fr
Ahmed.Loukili@ec-Nantes.fr

Key words: Microindentation, 3D microscopy, mechanical properties, irradiations, damage and creep.

Abstract: In this study, the combination of microindentation and 3D optical microscopy is studied to determine the mechanical properties of the cement pastes of pristine and irradiated mortars. It is shown that using optical microscopy information on top of statistical indentation technique and classification algorithms, the disadvantages of both techniques can be partly reduced and the mechanical properties attributed to the cement paste are refined. That way, some insights on the degradation mechanisms of dry cementitious materials under low dose γ-irradiations have been proposed, e.g. a significant increase of the hardness and the creep modulus after 257 kGy, which means that irradiated cement paste creeps less than pristine ones.

1 INTRODUCTION

For some years, microindentation and nanoindentation have been widely investigated to characterize elasto-plastic and creep properties of cementitious materials [1, 2]. Indentation elastic parameters can then be input in homogenization schemes to determine concrete elastic properties [3, 4]. Because cement paste is highly heterogenous, even at very small length scales, statistical nanoindentation performed at loads leading to penetration depths of some hundreds of nanometers has been developed. Assuming several phases may be indented at the same time, statistical indentation's main objective is to collect enough data points to apply a deconvolution algorithm giving the individual phase properties [5, 6]. However, two main critical aspects were identified regarding the application of statistical indentation technique to cementitious materials [7]: the size of the interaction volume may be larger than the size of the single phases at the risk of creating spurious peaks in the probability density function (PDF) as well as micromechanical values depending on the applied load, and the deconvolution analysis based on Gaussian Mixture itself may converge to local minima. Therefore, coupling indentation results to other techniques identifying the effective nature of the indents is of great interest at different scales: using atomic force microscope [8] or SEM [3]. Coupling nanoindentation and SEM-EDS to filter data points, Chen et al. highlighted the presence of ultra-high density CSH/$Ca(OH)_2$ nanocomposites in low water-to-cement ratio cement paste by correlating

micromechanical properties, e.g. indentation hardness or indentation modulus, to the portlandite volume fraction measured in volumes with approximately the same size as the one investigated through nanoindentation. Localization of indents by imaging techniques can also be used to differentiate the properties of several inclusions [9] and eventually map a restricted area depending on the measured mechanical properties [10]. From the microscale to the macroscale, 3D image analysis of concrete or mortar surface appears to offer a promising field of research for purposes of generating geometric or topological data and supplementing other experimental techniques or providing input for numerical models [11].

The main objective of the present work is to demonstrate the potential of two complementary methods, namely statistical microindentation and microscopy, which can be combined to detect hidden data trends. An application to the determination of mechanical properties of γ-irradiated mortars is then proposed. The first micro mechanical dataset of this type is reported and compared with the only measurement performed on concrete at a macroscopic scale some decades ago [12]. Hundreds of measurement points obtained from 3 irradiated and 3 pristine control specimens are compared to highlight hidden trends due to radiation exposure.

2 MATERIALS AND METHODS

2.1 Mortar specimens preparation and irradiation

Mortar specimens with dimensions of with dimensions of 4 x 4 x 16 cm^3 were prepared using 566 kg/m^3 of CEMI 52.5 Portland cement, 270 kg/m^3 of water, 1344 kg/m^3 of calcareous sand. After water curing during 28 days, the specimens were dried 14 days at a temperature of 45°C. Then half of the specimens (3 specimens) were irradiated in an irradiator at ARRONAX (137Cs source, 661 keV, 123.4 TBq) during 3 weeks up to a total dose of around 257 kGy while the other half (3 specimens) was kept in the same room outside of the irradiator. Several mechanical and chemo-physical tests were performed on these mortars and on other series as well. The results have been presented in some articles [13, 14] and reveal macroscopic mechanical evolutions which can hardly be explained. In the sake of clarity, some results may be evocated in regards to micromechanical results presented herein. No evident carbonation, pore size evolution or hydrated phases transformations were measured. Thus micromechanical properties evolutions may not be attributed to calcite formation as opposed to other studies [15].

2.2 Indentation setup and theory

After the irradiation period, indentation tests were performed the week after irradiation on the irradiated and the pristine specimens. A 2 x 2 cm^2 section was polished with Si-C paper with decreasing particle size (500, 1200, 2000, 4000) using ethanol as polishing liquid. Polishing times were selected around some minutes per paper to limit the risk of aggregate cracking.

Microindentation was performed using a Vickers indenter probe over a grid of 20 x 20 points, evenly spaced by 500 µm to investigate a representative surface of 1 x 1 cm^2 of the mortar sample. For each indent, the load was increased linearly over time in 5 s up to 2000 mN, kept constant during the 60 s holding phase, and decreased linearly over time back to zero in 5 s. The very short loading time was selected to limit creep during this period and do not apparently damaged the sample. Typical loading curves obtained during the test are represented on Fig. 1.

Various properties were calculated from the load – penetration curves. First, the indentation hardness H_{IT} depending on the maximum load P_{max} and the projected contact area A_p:

$$H_{IT} = \frac{P_{max}}{A_p(h_c)} \quad (1)$$

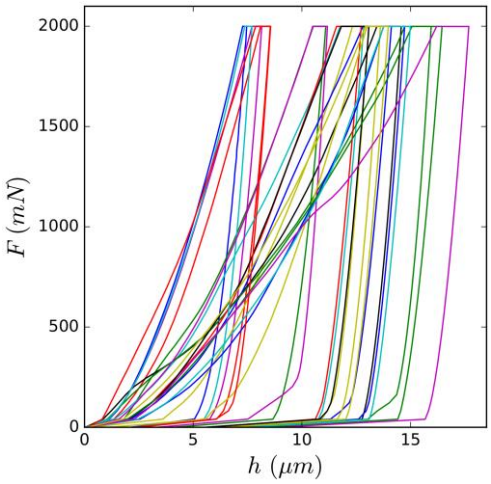

Figure 1: Selected indentations curves obtained on mortar specimens.

The Young's modulus EIT of the indented material is given by:

$$M = \frac{E_{IT}}{1-\nu_s^2} = \frac{1}{\frac{1}{E_r} - \frac{1}{M_{ind}}} \quad (2)$$

Where M denotes the indentation modulus, Mind = 1140 GPa the modulus of the indenter, ν_s the Poisson ratio of the material (considered equal to 0.2) and E_r is the reduced modulus which is determined assuming:

$$E_r = \frac{1}{2}\left(\frac{dP}{dh}\sqrt{\frac{\pi}{A}}\right) \text{ at } h = h_{max} \quad (3)$$

A first creep parameter C_{IT}, e.g. the normalized indentation creep parameter, was calculated by the machine. It is defined as:

$$C_{IT}(\%) = \frac{h_{max} - h_1}{h_1} \times 100 \quad (4)$$

More meaningful creep parameters C and τ can be extracted from the indentation curves calculating the creep function L(t) [10]:

$$L(t) - L(0) = L(t) - \frac{1}{M} = \frac{2a_u \Delta h(t)}{P_{max}} \quad (5)$$

Where Δh(t) denotes the indentation depth increase during the constant load phase, au denotes the is the radius of the equivalent projected contact area between the indenter probe and the indented surface at the onset of unloading

Assuming a logarithmic fit of the creep function, the creep parameters are defined according to [16]:

$$L(t) - \frac{1}{M} = \frac{\ln(t/\tau + 1)}{C} \quad (6)$$

This law can adequately reproduce the creep behavior of both cement paste and sand as illustrated in Fig. 2.

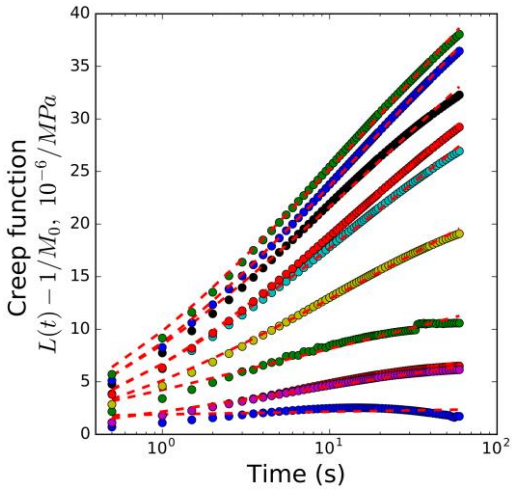

Figure 2: Microindentation creep function curve fitting using logarithmic law.

2.3 3D microscope measurements and analysis

After indentation, a map of the indented zone was realized using a Hirox RH-2000 3D microscope using a x 140 magnification leading to a final horizontal resolution of the 2D projected image of 1.5 µm / pix. A basic routine was implemented in Python to locate all the indents based on the location of 3 of them by drawing blue squares on the original image as illustrated in Fig. 3. The location of the indents were then manually identified and classified into one of the four categories: cement paste, sand, interface or void.

3 RESULTS AND DISCUSSION

3.1 Statistical indentation limits

First, indentation outputs from each specimen were visualized by mean of a scatter plot. Isolated points corresponding to voids or irregularities were removed before further analysis. Two main groups can be observed using the cumulative distributions of the main micromechanical parameters. In order to better classify the data points, hierarchical clustering

was performed using an Euclidian-based distance. An example of an obtained dendrogram for one specimen is represented on Fig. 4.

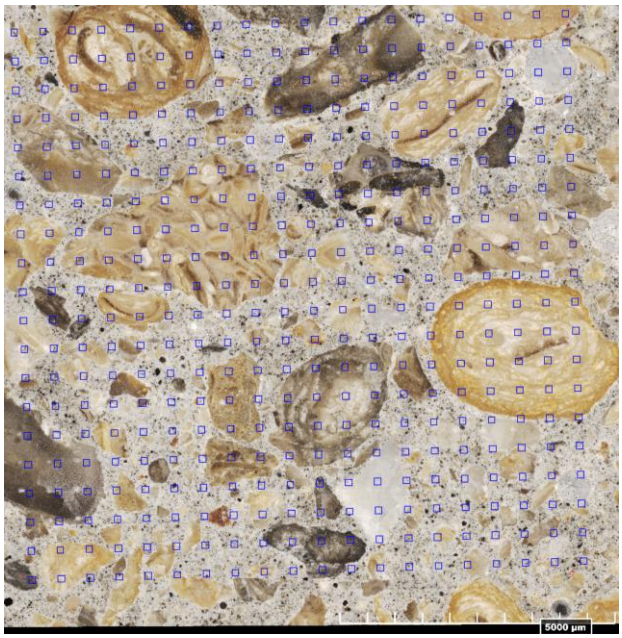

Figure 3: 2D projected global view of the 20 x 20 matrix of indents over a 1 x 1 cm² surface from 3D microscope acquisition (indents are indicated by blue squares).

Using dendrograms-cutoff at various heights, several groups may be obtained. The 2 major groups clearly separate cement paste indents and indents nearby sand particles while higher order groups make smaller distinctions. Cutting the dendrogram at a high of 20 leads to a 3-groups classification as illustraded by Fig. 5.

Reporting the nature of the indents predicted by deconvolution over the microscopic image as illustrated in Fig. 6, a relatively good correspondence is noticeable: red squares corresponding to the first deconvoluted group are mainly located in the paste and blue ones, corresponding to the second group are mainly located in sand grains, while black squares, corresponding to initially filtered values are all near voids. However, some indents numerically identified as cement paste are located on sand grains and vice versa which emphasizes the limits of numerical clustering.

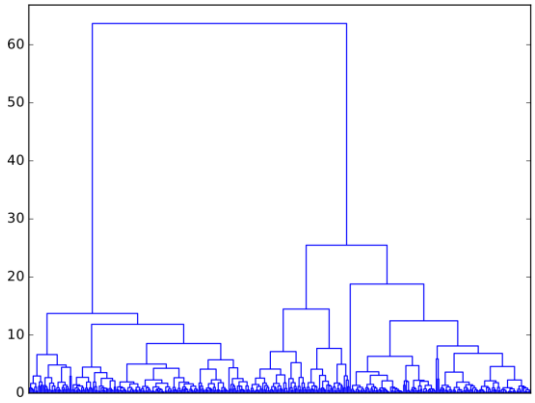

Figure 4: Euclidian-based distance dendrogram obtained using hierarchical clustering algorithms on one specimen indentation data set.

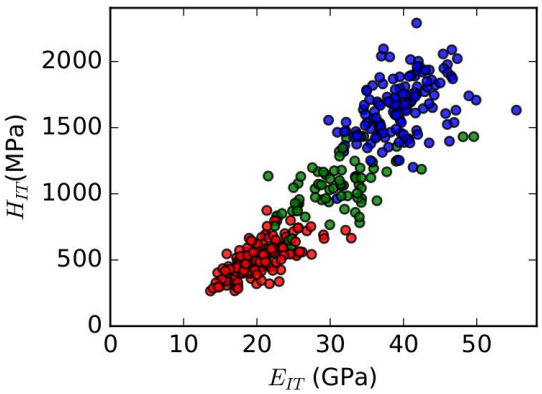

Figure 5: Data points repartition along C-H_{IT} plane using a 2-groups hierarchical clustering separation.

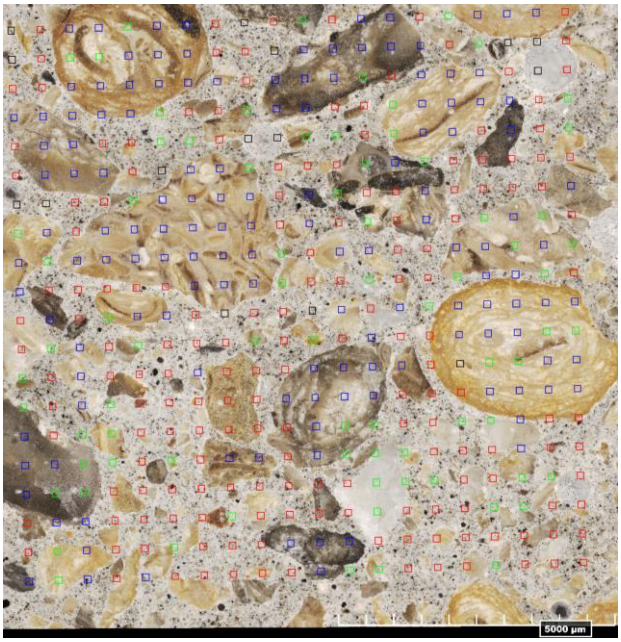

Figure 6: Representation on the 3D microscopic image of the nature of the indents predicted by data deconvolution (red squares correspond to group 1, e.g. ‘paste’, blue squares to group 2, e.g. ‘sand, and black squares to suppressed values).

3.2 3D microscope results

The selected parameters and magnification allowed a quick and relatively easy identification of the indent locations. The identified natures of the indents were close to those predicted using clustering algorithms. However one may note that there is an important proportion of indents located at the cement paste - sand grains interface. This is directly correlated to the indent size relatively to the size of the phase and the volume fraction of sand. This feature may be overcome using smaller loads but higher loads were selected to allow mainly for showing the generality of the proposed coupling technique alongside making sample preparation and quantification faster and results more reproducible with no influence of the roughness.

3.3 Combination of 3D microscope and indentation results

3D microscope and indentation data deconvolution phase assignations were combined to reduce the variability of the identified phase properties. Comparing the indent natures from the two first order techniques, the indents with corresponding natures were considered as representative of a given phase while the others were considered as non-reliable information.

A detailed analysis of the microindentation output variables through histograms (Fig. 7) reveals that non-corresponding indents are mainly the ones with intermediate properties as predicted by the visual observation. Interestingly, the initial goal of this comparison method seems to have been achieved: cement paste and sand distributions are tightened and do not overlap for Young's modulus, hardness and creep modulus.

From a visual inspection of the spatial repartition of the nature of the indents in one of the worst cases (Fig. 8), it should be observed that there is a huge proportion of noncorresponding indentss (yellow squares). Indeed, when comparing 3 groups from 3D microscope identification and 3 groups from data deconvolution, around 35% of indents nature do not correspond between the two analysis, while this proportion is usually around 25% for the comparison between 3 groups from 3D microscope and 2 groups from data deconvolution.

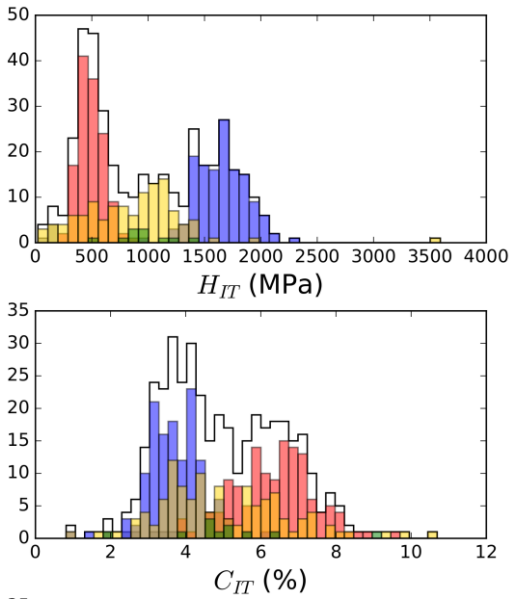

Figure 7: Histograms of distributions of the indentation output variables of one specimen after the combined use of numerical and clustering and image analysis. Total distribution is represented by the continuous black line, distributions of the phases are colored in red (cement paste), blue (sand grains), green (sand grain – cement pastes interface). The distribution of non-corresponding indents is represented in yellow.

A majority of noncorresponding indents are located in sand grains or at their periphery and this is the reason explaining why there is less error using 2 groups data from deconvolution data: data points numerically identified as belonging to the intermediate group were mostly visually identified as sand grains and not sand grain – cement paste interface. Only a very few indents were identified as interfaces by combining the two methods which means that groups identified by clustering algorithms with intermediate properties are not necessarily different phases (here sand grain – cement paste interface).

Figure 8: Representation on the 3D microscopic image of the nature of the indents predicted by coupling clustering algorithm and imùage analysis (red squares correspond to group 1, e.g. 'paste', blue squares to group 2, e.g. 'sand, and black squares to suppressed values)..

3.4 Application on low dose γ-irradiated mortars

Using the aforementioned method coupling statistical indentation and 3D image analysis, cement paste properties of pristine and irradiated mortar specimens were compared precisely and the evolution of the creep properties were assessed for the first time using micromechanical tests. Tables 1 and 2 summarize the results obtained using statistical indentation data clustering technique alone and using the method coupling statistical indentation data clustering and image analysis respectively.

Table 1: Indentation outputs for cement paste indents identified using hierarchical clustering: mean values and variances in brackets

	EIT (GPa)	HIT (MPa)	C (GPa)
Pristine 0 kGy	20.4 (14.4)	420.2 (14600)	168 (3539)
Irradiated 257 kGy	20.7 (18.2)	456.2 (17314)	196 (4998)

It may be observed a small increase of the Young's modulus and creep modulus of irradiated cement pastes while a more important increase of hardness is noticeable. These results obtained from hundreds of data points correlate well with the historical and only up-to-date observation of the influence of γ-irradiations on concrete made at a macroscopic level [12]. However, the standard deviation of the results is important so no statistically significant conclusion can be drawn.

Table 2: Indentation outputs for cement paste indents identified using the proposed method coupling numerical clustering and image analysis: mean values and variances in brackets

	EIT (GPa)	HIT (MPa)	C (GPa)
Pristine 0 kGy	19.7 (12.0)	406.1 (11455)	150 (1639)
Irradiated 257 kGy	19.8 (12.7)	428.8 (11226)	176 (2723)

The results from the coupled method are more precise as illustrated by Table 2: the variances of all the calculated values are clearly smaller compared to the variances of the same values computed using hierarchical clustering or statistical calculations based on the manual identification of the indents using 3D images. Considering these values, the increase of the hardness and the creep modulus of the cement paste of the mortars specimens irradiated by γ-rays after being dried is significant.

4 CONCLUSIONS AND PERSPECTIVES

In this paper, a novel method coupling statistical microindentation and 3D microscope image analysis has been proposed to reduce the variability of the micromechanical properties associated to an indented phase. This method relies on the comparison of the nature of indents numerically predicted by statistical indentation data deconvolution and by 3D-optical microscope image analysis. This method robustly counteracts the uncertainty of numerical clustering methods by introducing optical information. Using this method cement paste properties of pristine and irradiated mortar specimens were obtained. It has been found out that creep modulus C significantly

increases by around 17%. The creep modulus increase is correlated with a slight increase of the indentation hardness H_{IT}. On the other hand, Young's modulus of irradiated specimens does not significantly differ from the one of control specimens.

REFERENCES

[1] Trtik, P., Bartos, P.J.M., 1999. Micromechanical properties of cementitious composites. Mater. Struct. **3**: 388-93.

[2] Constantinides, G., Ulm, F.-J., Van Vliet, K., 2003. On the use of nanoindentation for cementitious materials. Mater. Struct. **36**: 191-96.

[3] Chen, J.J., Sorelli, L., Vandamme, M., Ulm, F.-J., Chanvillard, G., 2010. A Coupled Nanoindentation/SEM-EDS Study on Low Water/Cement Ratio Portland Cement Paste: Evidence for C-S-H/Ca(OH)2 Nanocomposites. J. Am. Ceram. Soc. **93**: 1484-93.

[4] Vandamme, M., Ulm, F.-J., 2013. Nanoindentation investigation of creep properties of calcium silicate hydrates. Cem. Concr. Res. **52**: 38-52.

[5] Ulm, F.-J., Vandamme, M., Bobko, C., Ortega, J.A., Tai, K., Ortiz, C., 2007. Statistical Indentation Techniques for Hydrated Nanocomposites: Concrete, Bone, and Shale. J. Am. Ceram. Soc. **90**: 2677-92.

[6] Sorelli, L., Constantinides, G., Ulm, F.-J., Toutlemonde, F., 2008. The nano-mechanical signature of Ultra High Performance Concrete by statistical nanoindentation techniques. Cem. Concr. Res. **38**: 1447-56.

[7] Hu, C., Gao, Y., Zhang, Y., Li, Z., 2016. Statistical nanoindentation technique in application to hardened cement pastes: Influences of material microstructure and analysis method. Constr. Build. Mater. 1**13**: 306-16.

[8] Mondal, P., Shah, S.P., Marks, L., 2007. A reliable technique to determine the local mechanical properties at the nanoscale for cementitious materials. Cem. Concr. Res. **37**: 1440-44.

[9] Zhao, S., Sun, W., 2014. Nano-mechanical behavior of a green ultra-high performance concrete. Constr. Build. Mater. **63**: 150-60.

[10] Vandamme, M., Ulm, F.-J., Fonollosa, P., 2010. Nanogranular packing of C-S-H at substochiometric conditions. Cem. Concr. Res. **40**: 14-26.

[11] Hilloulin, B., Legland, J.-B., Lys, E., Abraham, O., Loukili, A., Grondin, F., Durand, O., Tournat, V., 2016. Monitoring of autogenous crack healing in cementitious materials by the nonlinear modulation of ultrasonic coda waves, 3D microscopy and X-ray microtomography. Constr. Build. Mater. **123**: 143-52.

[12] McDowall, D. The effects of gamma radiation on the creep properties of concrete. In Proceedings of the Information Exchange Meeting on 'Results of Concrete Irradiation Programs', EUR 4751 f-e, Commission des Communautés Européennes, Brussels, Belgium, 1971

[13] Hilloulin, B., Robira, M., Loukili, A., 2018. Coupling statistical indentation and microscopy to evaluate micromechanical properties of materials: Application to viscoelastic behavior of irradiated mortars. Cem. Concr. Compos. **94**: 153-65.

[14] Robira, M., Hilloulin, B., Loukili, A., Potin, G., Bourbon, X., Abdelouas, A., 2018. Multi-scale investigation of the effect of γ irradiations on the mechanical properties of cementitious materials. Constr. Build. Mater. **186**: 484-94.

[15] Vodák, F., Vítězslav, V., Trtík, K., Kapičcková, O., 2011. Effect of gamma irradiation on properties of hardened cement paste. Mater. Struct. **44**: 101-07.

[16] Zhang, Q., Roy, R. Le, Vandamme, M., Zuber, B., 2014. Long-term creep properties of cementitious materials: Comparing microindentation testing with macroscopic uniaxial compressive testing. Cem. Concr. Res. **58**: 89-98.